The Community Climate System Model Version 4

PETER R. GENT,* GOKHAN DANABASOGLU,* LEO J. DONNER,+ MARIKA M. HOLLAND,* ELIZABETH C. HUNKE,# STEVE R. JAYNE,@ DAVID M. LAWRENCE,* RICHARD B. NEALE,* PHILIP J. RASCH,& MARIANA VERTENSTEIN,* PATRICK H. WORLEY,** ZONG-LIANG YANG,++ AND MINGHUA ZHANG##

* *National Center for Atmospheric Research, Boulder, Colorado*
+ *Geophysical Fluid Dynamics Laboratory, Princeton, New Jersey*
# *Los Alamos National Laboratory, Los Alamos, New Mexico*
@ *Woods Hole Oceanographic Institution, Woods Hole, Massachusetts*
& *Pacific Northwest National Laboratory, Richland, Washington*
** *Oak Ridge National Laboratory, Oak Ridge, Tennessee*
++ *University of Texas, Austin, Texas*
Stony Brook University, Stony Brook, New York

(Manuscript received 20 September 2010, in final form 1 April 2011)

ABSTRACT

The fourth version of the Community Climate System Model (CCSM4) was recently completed and released to the climate community. This paper describes developments to all CCSM components, and documents fully coupled preindustrial control runs compared to the previous version, CCSM3. Using the standard atmosphere and land resolution of 1° results in the sea surface temperature biases in the major upwelling regions being comparable to the 1.4°-resolution CCSM3. Two changes to the deep convection scheme in the atmosphere component result in CCSM4 producing El Niño–Southern Oscillation variability with a much more realistic frequency distribution than in CCSM3, although the amplitude is too large compared to observations. These changes also improve the Madden–Julian oscillation and the frequency distribution of tropical precipitation. A new overflow parameterization in the ocean component leads to an improved simulation of the Gulf Stream path and the North Atlantic Ocean meridional overturning circulation. Changes to the CCSM4 land component lead to a much improved annual cycle of water storage, especially in the tropics. The CCSM4 sea ice component uses much more realistic albedos than CCSM3, and for several reasons the Arctic sea ice concentration is improved in CCSM4. An ensemble of twentieth-century simulations produces a good match to the observed September Arctic sea ice extent from 1979 to 2005. The CCSM4 ensemble mean increase in globally averaged surface temperature between 1850 and 2005 is larger than the observed increase by about 0.4°C. This is consistent with the fact that CCSM4 does not include a representation of the indirect effects of aerosols, although other factors may come into play. The CCSM4 still has significant biases, such as the mean precipitation distribution in the tropical Pacific Ocean, too much low cloud in the Arctic, and the latitudinal distributions of shortwave and longwave cloud forcings.

1. Introduction

The Community Climate System Model (CCSM) is a general circulation climate model consisting of atmosphere, land, ocean, and sea ice components that are linked through a coupler that exchanges state information and fluxes between the components. The CCSM is developed and used by a community of scientists and students from universities, national laboratories, and other institutions. The CCSM has been used to study several paleoclimate epochs, the climate of the more recent past, and to make projections of possible future climate change. The most recent version, CCSM4, was made available to the community on 1 April 2010 from the CCSM Web site (http://www.cesm.ucar.edu/models/ccsm4.0/). The code, a reference manual, and a user's guide for each component, the input datasets, and the output from some standard model simulations are freely available. This overview paper describes some of the most important developments and improvements in the

Corresponding author address: Peter R. Gent, NCAR, P.O. Box 3000, Boulder, CO 80307.
E-mail: gent@ucar.edu

DOI: 10.1175/2011JCLI4083.1

model components and the simulated climate of the recent past using CCSM4 compared to results from CCSM3. Other papers in the CCSM4 Special Collection describe the components in much more detail, and focus on particular phenomena or aspects from the preindustrial and twentieth-century runs. A few papers document projections of possible future climate change over the twenty-first century using results from CCSM4.

The first version of the CCSM, called the Climate System Model, was released in 1996 (Boville and Gent 1998) and was the first climate model that could maintain a stable present-day simulation without the use of flux corrections. The CCSM2 was released in 2002 (Kiehl and Gent 2004), and CCSM3 was released in June 2004 (Collins et al. 2006). One of the worst aspects of the CCSM3 climate was the El Niño–Southern Oscillation (ENSO) period, which was dominated by variability at 2 yr, rather than the 3–7-yr period from observations. Improving ENSO was the highest priority in CCSM4 development, and a significant improvement has been achieved. The ENSO period was made much more realistic by two changes to the deep convection parameterization in the atmosphere component (Richter and Rasch 2008; Neale et al. 2008). An interim version, CCSM3.5 (Gent et al. 2010), including these changes was not formally released, but has been available to many researchers involved with the project. This very important improvement to the simulation of ENSO is retained in CCSM4 and is documented below in section 5d.

The CCSM4 is one of many climate models being finalized around the world to participate in the Coupled Model Intercomparison Project's fifth phase (CMIP5). The CMIP5 protocol calls for long projection runs for the remainder of the twenty-first century without and with an interactive carbon cycle, and for a set of decadal prediction runs where the ocean component is initialized to observations in some fashion. Results from these runs using CCSM4 and the other climate models will be submitted to the Intergovernmental Panel on Climate Change (IPCC) for inclusion in the fifth Assessment Report, scheduled for publication in 2013.

This CCSM4 overview paper documents coupled runs where the atmosphere and land components use finite volume grids with resolutions near 1° and 2°. Both resolutions are coupled to the same nominal 1° versions of the ocean and sea ice components. A lower-resolution version of CCSM4, suitable for paleoclimate studies, is documented in Shields et al. (2011, manuscript submitted to *J. Climate*). Section 2 briefly documents the major developments in all CCSM components since the previous released version, CCSM3. Section 3 is a description of the strategy used to produce the preindustrial control and twentieth-century runs, and details of how these runs are forced. Sections 4–7 show results from long preindustrial control runs using both the 1° and 2° resolutions in the atmosphere and land components and from an ensemble of twentieth-century runs using 1° atmosphere and land resolution. These runs are compared to available observations and comparable runs using CCSM3. Section 8 contains the conclusions and a summary of both the improvements and some of the most important biases remaining in CCSM4 simulations.

2. Overview of the CCSM4

The core of the Community Atmosphere Model (CAM4) changed from the spectral core used in CAM3 to the Lin–Rood finite volume core (Lin 2004). Aspects of the polar filtering in this core have been changed, which eliminated a minor problem in fields where the filtering started and considerably reduced the level of numerical noise. Changes were made to the deep convection scheme by including the effects of deep convection in the momentum equation (Richter and Rasch 2008) and using a dilute, rather than an undilute, approximation in the plume calculation (Neale et al. 2008). These changes resulted in a much improved representation of deep convection that occurs considerably less frequently, but is much more intense in CAM4 compared to CAM3. A freeze-dry modification was added to the low cloud parameterization (Vavrus and Waliser 2008), which has the effect of reducing the amount of wintertime low cloud in the Arctic region, although the amount is still too large compared to observations. The Froude number coefficient in the gravity wave parameterization was retuned, which improved the CAM4 simulation in the upper atmosphere. The horizontal grid used is latitude/longitude with 288×200 points, resulting in a uniform resolution of $1.25° \times 0.9°$ in the 1° version, and half the number of grid points in both directions in the 2° version. CAM4 uses 26 layers in the vertical, which are distributed similarly to CAM3. The CAM4 is documented in R. B. Neale et al. (2011, unpublished manuscript).

There have been several developments to the CCSM4 ocean component, which uses the Parallel Ocean Program version 2 (Smith et al. 2010). How the parameterization for the effects of mesoscale eddies transitions from the nearly adiabatic deeper ocean to the well-mixed surface layer has been much improved (Danabasoglu et al. 2008). The thickness and isopycnal diffusivity coefficients are now functions of space and time, and are much larger in the upper ocean than the deep ocean (Danabasoglu and Marshall 2007). This vertical decay is a much more realistic representation of ocean eddy energy than the constant values specified in CCSM3. The anisotropic horizontal viscosity parameters have been

changed so that the viscosity is now substantially smaller, especially near the equator and the western boundaries of ocean basins (Jochum et al. 2008). This allows the tropical instability waves in the tropical Pacific to be much more energetic and realistic. The vertical mixing terms now have a term that is proportional to the tidal energy (Jayne 2009), which allows a little more cross-isopycnal mixing in the deep ocean. A new parameterization for the effects of submesoscale eddies (Fox-Kemper et al. 2008) has been included that helps to restratify the ocean mixed layer. Finally, a new parameterization for deep ocean overflows, such as the Denmark Strait and Faroe–Scotland Ridge in the North Atlantic, has been implemented (Danabasoglu et al. 2011b). This improves the penetration of overflow water into the very deep ocean, which has been a long-standing problem of models that use depth coordinates. The nominal 1° grid uses spherical coordinates in the Southern Hemisphere, but in the Northern Hemisphere the pole is displaced into Greenland at 80°N, 40°W. The horizontal grid has 320×384 points, and the resolution is a uniform 1.11° in the zonal direction. The meridional resolution is 0.27° around the equator, gradually increasing to 0.54° at 33°N/S, and is constant at higher latitudes. There are now 60 vertical levels, as opposed to 40 in CCSM3, with the number of 10-m levels in the upper ocean increased to 20. The ocean component is documented in Danabasoglu et al. (2011a, hereafter D11a).

An interim version of the Community Land Model (CLM3.5) was released in 2008 and is documented in Oleson et al. (2008) and Stockli et al. (2008). Compared to CLM3 there were changes to several parts of the model hydrology, such as the surface runoff, the groundwater scheme, and the frozen soil scheme. Other new features were a revised canopy integration, canopy interception scaling, and a plant functional type dependency on the soil moisture stress function. CLM3.5 had a much improved representation of evapotranspiration and the annual cycle of water storage compared to CLM3.

Many additional capabilities, input datasets, and parameterization updates have been included in the CLM4 (Lawrence et al. 2011a). It includes a carbon–nitrogen (CN) cycle component that is prognostic in carbon and nitrogen as well as vegetation phenology (Thornton et al. 2007), though the carbon and nitrogen fluxes are purely diagnostic and are not passed to the atmosphere. However, the CN component does have an impact on climate because the seasonal and interannual vegetation phenology (i.e., leaf area index and vegetation height) is prognostic. The dynamic global vegetation model (DGVM) has been expanded to include temperate and boreal shrub vegetation types and is merged with CN such that the carbon dynamics are controlled by CN while the dynamic vegetation biogeography aspects of the CLM3 DGVM are retained. CLM4 also has a transient land cover and land-use change capability, including wood harvest, and a new urban component. The biogenic volatile organic compound emissions component is replaced with the Model of Emissions of Gases and Aerosols from Nature (MEGAN2) (Heald et al. 2008). The hydrology scheme is further updated, and the ground evaporation now accounts for litter and within-canopy stability. The Snow and Ice Aerosol Radiation (SNICAR) model (Flanner and Zender 2006) has been included, as well as new snow cover fraction, snow burial of vegetation, and snow compaction parameterizations. To improve the representation of permafrost, the thermal and hydrologic properties of organic soil are accounted for, and the ground column is extended to 50-m depth by adding five bedrock layers. The plant functional type distribution is as in Lawrence and Chase (2007), except with a new cropping dataset. The river discharge has been separated into liquid and ice water streams. Heat from the ocean component is required to melt the ice and this has improved the global heat conservation of CCSM4. The CLM4 uses the same horizontal grid as the atmosphere component. Assessment of the land surface climate simulation and the impact of new land component capabilities are documented in Lawrence et al. (2011b, manuscript submitted to *J. Climate*).

The CCSM4 sea ice component is based on the Community Ice Code version 4 (Hunke and Lipscomb 2008), which includes the improved ridging scheme of Lipscomb et al. (2007). The most important developments compared to the CCSM3 version are the incorporation of a new radiative transfer scheme (Briegleb and Light 2007) and the new capabilities that this allows. The delta-Eddington radiative transfer makes use of inherent optical properties to define the scattering and absorption characteristics of snow, sea ice, and included absorbers. It explicitly allows for the incorporation of melt ponds and absorbers, such as black carbon and dust, in the radiation physics. Therefore, a relatively simple melt pond parameterization is incorporated that simulates the pond volume and area as a function of the surface meltwater flux, and aerosol deposition and cycling on sea ice are also included. Taken together, these improvements allow for a more sophisticated, internally consistent, and complete treatment of the surface albedo and shortwave radiative transfer in the ice and overlying snowpack. The CCSM4 uses much more realistic surface ice albedos than the low values used in CCSM3. The sea ice component uses the same horizontal grid as the ocean component. These new capabilities, and their impacts on the simulated climate, are discussed in Holland et al. (2011, hereafter H11).

The CCSM4 has a completely new coupling infrastructure, CPL7, that consists of a single executable design that provides flexibility in running CCSM components sequentially, concurrently, or in a mixed sequential–concurrent mode. This flexibility is achieved through the introduction of a top-level driver that runs on every computer processor and controls the time sequencing, processor concurrency, and exchange of state information and fluxes between components. In CPL7, all model components and the coupler itself can run on potentially overlapping processor subsets. This design permits the model system to have greatly increased flexibility to achieve the model component layout that optimizes the overall performance and efficiency of the model. The CCSM4 also includes a new scripting system that permits the user to easily specify the processor layout of the model components, and is also accompanied by informative timing utilities. Together, these tools enable a user to create a wide variety of ''out of the box'' experiments for different model configurations and resolutions and also to determine the optimal load balance for those experiments to ensure maximum throughput and efficiency. The new CPL7 infrastructure is a significant advance on the CCSM3 coupler, where all components were constrained to run as separate executables on unique processor sets, and there was no concept of a top-level driver. CPL7 is documented online (http://www.cesm.ucar.edu/models/cesm1.0/cpl7/cpl7_doc/book1.html) and in Craig et al. (2011, manuscript submitted to *Int. J. High Perf. Comput.*).

The atmosphere, land, and sea ice components communicate both state information and fluxes through the coupler every atmospheric time step. The only fluxes still calculated in the coupler are those between the atmosphere and ocean, and the coupler communicates them to the ocean component only once a day. However, the important diurnal cycle in the upper tropical oceans is simulated as described in Danabasoglu et al. (2006). The daily net solar radiation is multiplied by a function that is zero at night, has a maximum value at midday, and integrates to one over the day. This conserves heat and allows buoyancy-driven vertical mixing to occur at night in the upper ocean. However, Danabasoglu et al. conclude that this method only produces a small rectification on the model SST compared to that found in Bernie et al. (2005). The main reason is that CCSM4 uses an upper-ocean resolution of 10 m compared to 1 m in the Bernie et al. (2005) model.

3. Preindustrial control and twentieth-century runs

In this section, the setup of preindustrial control and twentieth-century integrations of CCSM4 will be described, which used a strategy designed to address problems of energy balance and climate drift in CCSM3. For that model, most development effort went into producing a present-day control run, which was energetically well balanced at the top of the atmosphere (TOA) (Collins et al. 2006). The CCSM3 1870 preindustrial control run kept the same parameter values as the present-day control, but changed the forcings, which meant that the system lost heat at a rate of nearly 0.6 W m^{-2}. Thus, the entire ocean cooled in the CCSM3 1870 control run so that the total ocean heat content decreased very significantly. The CCSM3 twentieth-century runs were branched from this 1870 control, and the ocean heat content changes over the twentieth century had to be calculated with respect to the large drift in the 1870 control run (Gent et al. 2006). This strategy was less than optimal, and a different strategy was chosen for CCSM4. It was decided to concentrate on a preindustrial control run, and 1850, rather than 1870, was chosen because the carbon dioxide (CO_2) and aerosol concentrations are closer to preindustrial levels in 1850. A real disadvantage of this choice is that it is much harder to compare the long 1850 control run with observations. However, this is outweighed by the advantage of having more realistic twentieth-century runs, where the climate system, including the ocean component, is gaining heat.

The CCSM project uses the following strategy to produce control integrations. All four components are finalized independently by the respective working groups using stand-alone runs, such as Atmospheric Model Intercomparison Project integrations and runs of the individual ocean, land, or sea ice components forced by atmospheric observations. Once the components are coupled, then the only parameter settings that are usually allowed to change are the sea ice albedos and a single parameter in the atmosphere component. This is the relative humidity threshold above which low clouds are formed, and it is used to balance the coupled model at the TOA. A few 100-yr coupled runs are required to find the best values for these parameters based on the Arctic sea ice thickness and a good TOA heat balance. The rationale for this strategy is that the individual components need the best parameter values for the many integrations done in stand-alone mode, and it would be difficult to track using different values in stand-alone and coupled modes. In addition, it is thought to be inappropriate if changing a parameter value in one of the components is allowed to compensate for poor forcings or boundary conditions provided by the other components in coupled runs. The relative humidity threshold takes different values in the different resolution configurations described below, and final AMIP runs for each resolution are made using exactly the same parameter

values as in coupled mode. The resulting preindustrial run is integrated out for a few hundred years in order for the system, including the upper ocean, to come into equilibrium. Next, a twentieth-century run from 1850 to 2005 is completed, and a decision on whether this is acceptable is made based almost exclusively on two comparisons against observations. They are the globally averaged surface temperature against the historical reconstruction and the September Arctic sea ice extent from 1979 to 2005 against the satellite era observations. This second comparison is the reason that the sea ice albedos are allowed to change after the components are coupled. If these comparisons are deemed unacceptable, then the process of setting up the preindustrial control run would be repeated. Repetition takes a lot of time, mostly because of the time it takes to complete the integrations. With CCSM4, this setup procedure was repeated once early on with the 2°-resolution version. With the 1° version it was not repeated, even though the two comparisons described above are not quite as good as had been hoped, see section 7, but they were deemed as acceptable.

The original intention was to use 2° resolution in the atmosphere component for the standard, long climate change runs without and with a carbon cycle, and to use 0.5° resolution for the new, shorter decadal forecasts. This was based on the large improvements in sea surface temperatures (SSTs) in the major upwelling regions going from 2° to 0.5° atmosphere resolution in CCSM3.5, documented in Gent et al. (2010). However, it was found in CCSM4 that a majority of the upwelling region SST improvement between 2° and 0.5° resolution was obtained by using 1° atmosphere resolution; see section 4a. Given this SST improvement, and other benefits in the atmosphere simulation, it was decided to define 1° resolution as the CCSM4 standard and to use it for both the standard climate change runs and decadal forecasts. This increased the computer cost of the climate change runs, but decreased the cost of the decadal forecasts because using 1°, not 0.5°, atmosphere resolution cuts the computer cost of the entire model by a factor of 3. These decisions are always a delicate balance between possible further improvements due to increased resolution and the total computer time needed to accomplish all of the integrations asked for in the CMIP5 protocol.

The CCSM4 1850 control runs have the following forcings, which are kept constant during the runs. The incoming solar radiation at the TOA is 1360.9 W m^{-2}, and the CO_2 level is set to 284.7 ppm. Aerosol concentrations of sulfate, black and organic carbon, dust, and sea salt are specified from a historical run using the CCSM chemistry component with prescribed emissions (Lamarque et al. 2010), plus a low background level due to volcanic activity. The model was initialized with fields from the end of a previous short coupled run that had slightly different parameter settings. The 1° 1850 control was run for 1300 years, but some very small corrections were made during the run. At year 715, a small revision to the nitrogen deposition used in the CLM was introduced, along with very small changes to some constants in the ocean overflow parameterization. At year 851, a correction was made that fixed a small trend in the amount of aquifer water in the CLM, which changed the amount of river runoff reaching the ocean component, and made CCSM virtually conservative of freshwater. These corrections made almost no difference to the model climate. The 2° 1850 control run included the three corrections just described, and was run for 1000 years with no changes.

A TOA mean heat balance of $<|0.1|$ W m^{-2} in long control runs is always desirable. This means that there are only small drifts in the control run and the initial conditions for twentieth-century runs will be relatively realistic, even when taken from late in the control run. In contrast, if the control run drift is large, then the ocean conditions late in the run can become quite unrealistic. The CCSM4 preindustrial control runs did not quite meet this desired balance. The TOA heat balance started out at $<|0.1|$ W m^{-2} in the control runs, but worsened after about 100 yr, and the imbalance then remained almost constant for the remainder of the integrations. The 1° version lost heat at the TOA at a globally averaged rate of 0.147 W m^{-2} over years 601–1300, and this loss is almost constant with time. Most of the loss must come from the ocean component, which lost heat at a globally averaged rate of 0.098 W m^{-2}, while the land and sea ice components both lost heat at globally averaged rates of 0.035 and 0.014 W m^{-2}, respectively. Even though these heat loss rates look quite small, the globally averaged ocean temperature goes down from 3.55°C in the initial conditions to 3.13°C after 1300 yr. Analysis of the ocean solution shows that most of this loss does not come from the upper ocean, but from the depth range 1.5–3 km. Thus, the SST and upper-ocean heat content have very small drifts throughout the run after an initial period of adjustment, so the ocean drift only affects the sea ice distribution minimally. In the 2° version, the heat loss at the TOA is also fairly constant over the entire run, but the average is slightly smaller at 0.131 W m^{-2}. Again, this comes mostly from the ocean component, which lost heat at the rate of 0.084 W m^{-2}. The 1° run has a very small trend in ocean salinity because of the trend in the amount of aquifer water. However, the 2° run used the aquifer correction in the CLM throughout so that the minute increase in ocean salinity of 4×10^{-4} ppt over 1000 yr reflects a small increase in the volume of sea ice.

The CCSM4 twentieth-century runs begin in January 1850 and end in December 2005. They are forced by time series of solar output, greenhouse gases, several aerosols, and volcanic activity. The solar output anomaly time series is described in Lean et al. (2005) and is added to the 1360.9 W m^{-2} used in the 1850 control run. The CCSM4 volcanic activity is included by a time series of varying aerosol optical depths, exactly as in CCSM3 (Ammann et al. 2003). The CO_2 and other greenhouse gases (methane and nitrous oxide) are specified as in the IPCC third assessment report. Atmosphere aerosol burden (sulfate, organic carbon, and sea salt), aerosol deposition (black carbon and dust) onto snow, and nitrogen deposition also vary with time. The burdens and deposition rates were obtained from a twentieth-century run with the CCSM chemistry component active, which is forced with prescribed historical emissions (Lamarque et al. 2010). These concentrations do contain an annual cycle and are linearly interpolated in time from year to year within each month. This leads to a smoothly varying aerosol forcing compared to concentrations found in a fully interactive aerosol model. However, this probably does not affect the long-term trend and impact of these aerosols. Land cover changes in the CLM are prescribed on an annual basis according to a global historical transient land-use and land cover dataset (Hurtt et al. 2006). The initial conditions for the five members of the CCSM4 twentieth-century ensemble are taken from years 863, 893, 937, 983, and 1031 of the 1° 1850 control run, which were chosen to be after the last model correction and to span the range of variability in the North Atlantic meridional overturning circulation (MOC). The CCSM3 twentieth-century ensemble members were initialized from the 1870 control run at intervals of 20 yr starting at year 360, and no attention was paid to sampling the North Atlantic MOC variability.

4. Ocean and sea ice climatology

a. Sea surface temperature

The SST from these preindustrial control runs is one field that can be compared to observations from that time because the Hurrell et al. (2008) SST dataset goes back to 1870. The SST differences from observations in the 1° and 2° 1850 control runs from CCSM4 and the 1870 control run from CCSM3 are shown in Fig. 1. The globally averaged differences in these three runs are 0.07°, 0.30°, and −0.76°C, and the root-mean-square errors are 1.11°, 1.46°, and 1.57°, respectively, which shows the improvement in CCSM4 in this important measure compared to CCSM3. As noted above, CCSM3 SSTs are cold because the 1870 control run lost heat from the ocean at the rather significant rate of almost 0.6 W m^{-2}.

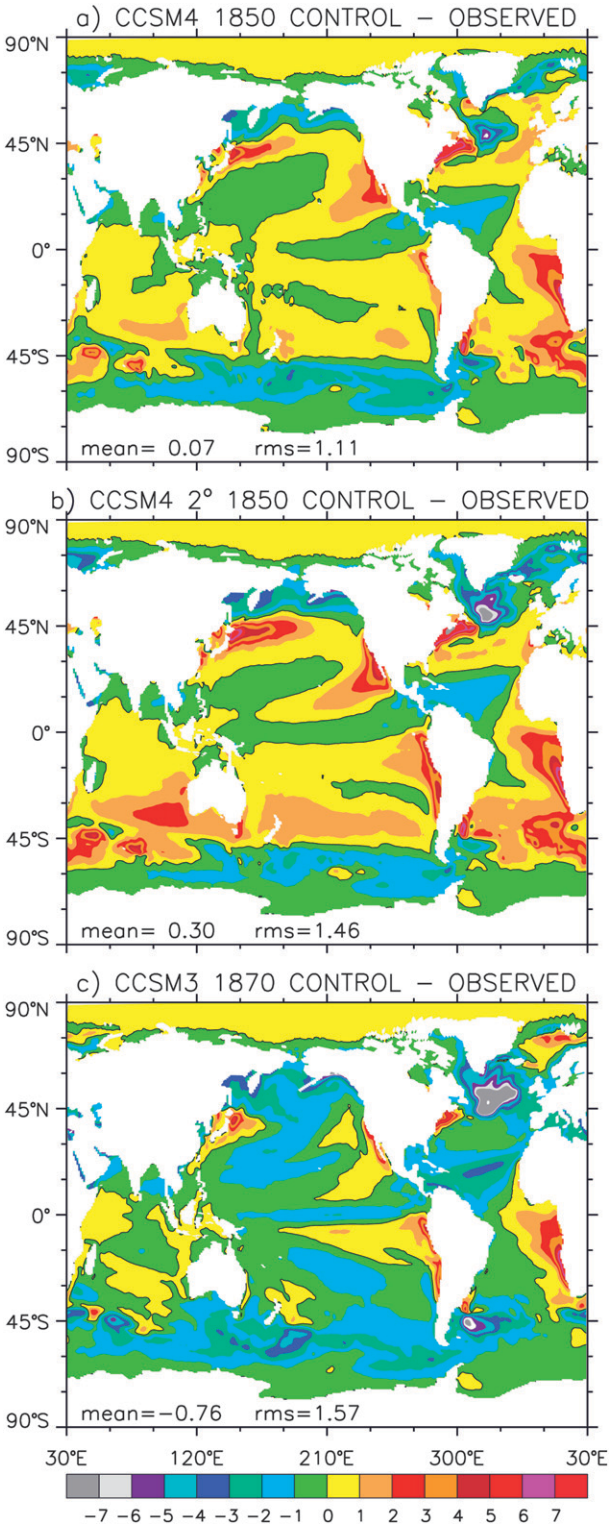

FIG. 1. Mean SST differences (°C) from the Hurrell et al. (2008) observations for the (a) CCSM4 1° 1850 control, (b) CCSM4 2° 1850 control, and (c) CCSM3 T85 1870 control. The observations use ⟨1870–99⟩ and all runs use ⟨871–900⟩, where the averaging period is indicated by angle brackets in this and following figure captions.

Figure 1 shows that CCSM4 improvement occurs in all oceans except the Arctic, with considerably larger regions having a difference between ±1°C in CCSM4. Figure 1 also shows that the large cold bias in the North Atlantic due to the Gulf Stream path being too far south is considerably reduced in CCSM4. This is due to the new overflow parameterization (Danabasoglu et al. 2011b) and other changes in the ocean component. Figures 1a and 1b show the reduced errors in the major upwelling regions and in the Southern Hemisphere midlatitudes when using 1° atmosphere resolution compared to 2° in CCSM4. The SST errors in the upwelling regions in the 1° version are comparable in both size and extent to CCSM3's 1870 control that used T85 truncation in the atmosphere spectral grid, which is a resolution of about 1.4°. The smaller mean SST bias and reduced upwelling region errors were the major reasons for choosing the 1° atmosphere resolution as the standard version for CCSM4 rather than the 2° version. Gent et al. (2010) analyze the reasons for these SST improvements in CCSM3.5, and the most important factor is that the finer resolution, and consequent better representation of topography, in the atmosphere component produces stronger upwelling favorable winds, which are located right along the model coasts rather than somewhat offshore.

b. Ocean meridional overturning circulation

Figures 2a and 2b show the MOC in the Atlantic Ocean from the CCSM3 1870 control run, and CCSM4 1850 control run. The MOC is calculated using just the mean velocity and does not include the eddy-induced velocity because that was not archived from CCSM3 runs. The CCSM3 1870 control run has a strong salinity trend in the deep ocean, so the earlier period was chosen to minimize the effect of this trend, which deepened the North Atlantic MOC. The maximum overturning occurs near 35°N at about 1-km depth and is stronger in CCSM4 at >24 sverdrups (Sv $\equiv 10^6$ m^3 s^{-1}) than the >20 Sv in CCSM3. The most striking effect of the new overflow parameterization is that the North Atlantic deep-water circulation reaches to the bottom of the ocean between 15° and 55°N in CCSM4, whereas it only reaches down to between 3 and 4 km at these latitudes in CCSM3. The deeper penetration of North Atlantic Deep Water has been thoroughly documented in Danabasoglu et al. (2011b). Figures 2c and 2d show the global MOC from CCSM3 and CCSM4. The first large difference in CCSM4 is the reduced MOC at 45°S in the region of the Antarctic Circumpolar Current, which is a result of weaker, more realistic, zonal wind stress driving the ocean at this latitude. This, and the smaller ocean viscosity, result in the mean transport through Drake Passage being reduced to 170 Sv in CCSM4, rather than the 205 Sv in CCSM3. The second large difference is the much weaker deep MOC in the Southern Hemisphere in CCSM4, with the value of nearly 8 Sv compared to 20 Sv in CCSM3 probably being more in line with the uncertain estimates from observations (Orsi et al. 1999). A contributing cause is that CCSM4 has slightly weaker offshore winds blowing over the ocean from the Antarctic continent in the Ross and Weddell Seas. This results in less sea ice drifting northward away from the coast and, consequently, less sea ice formation there. This reduces the brine rejection on the Ross and Weddell Sea shelves in CCSM4 compared to CCSM3, which is a primary cause of deep-water formation on the shelf and contributes to the deep MOC and northward flowing Antarctic bottom water.

c. Arctic sea ice concentration

Figure 3 shows the mean sea ice concentration in the Arctic from the CCSM4 1850 and CCSM3 1870 control runs, and the black lines are the 10% mean concentration values from recent Special Sensor Microwave Imager (SSM/I) satellite observations. The figure shows that the sea ice was much too extensive in the Labrador Sea and adjacent North Atlantic in CCSM3, and this is much improved in CCSM4 with the southern Labrador Sea being ice free. The main reason for this improvement is the smaller horizontal viscosity along all coasts in the ocean component (Jochum et al. 2008). This improvement means that deep-water formation can occur in the southern Labrador Sea in CCSM4, whereas it was incorrectly located farther east in the North Atlantic in CCSM3. The CCSM4 is also improved a little in the Barents Sea, but is a little worse east and north of Iceland, compared to CCSM3. The concentrations are comparable in the Arctic Ocean and North Pacific Ocean, and the sea ice thickness distributions are also comparable. In CCSM3 the reasonable sea ice distribution was obtained using rather low ice albedo values that were outside of the observed range. These low albedos compensated for the 40–50 W m^{-2} deficit of shortwave radiation at the surface in summer (Collins et al. 2006) caused by other biases such as the very poor Arctic low cloud amount. However, in CCSM4 this bias in summer downward shortwave radiation has almost been eliminated, and the albedo values used are higher and within the observational range (H11). The Antarctic sea ice distributions in CCSM3 and CCSM4 (not shown) are comparable and both are too extensive, but again the CCSM4 distribution is obtained using sea ice albedos within the observational range.

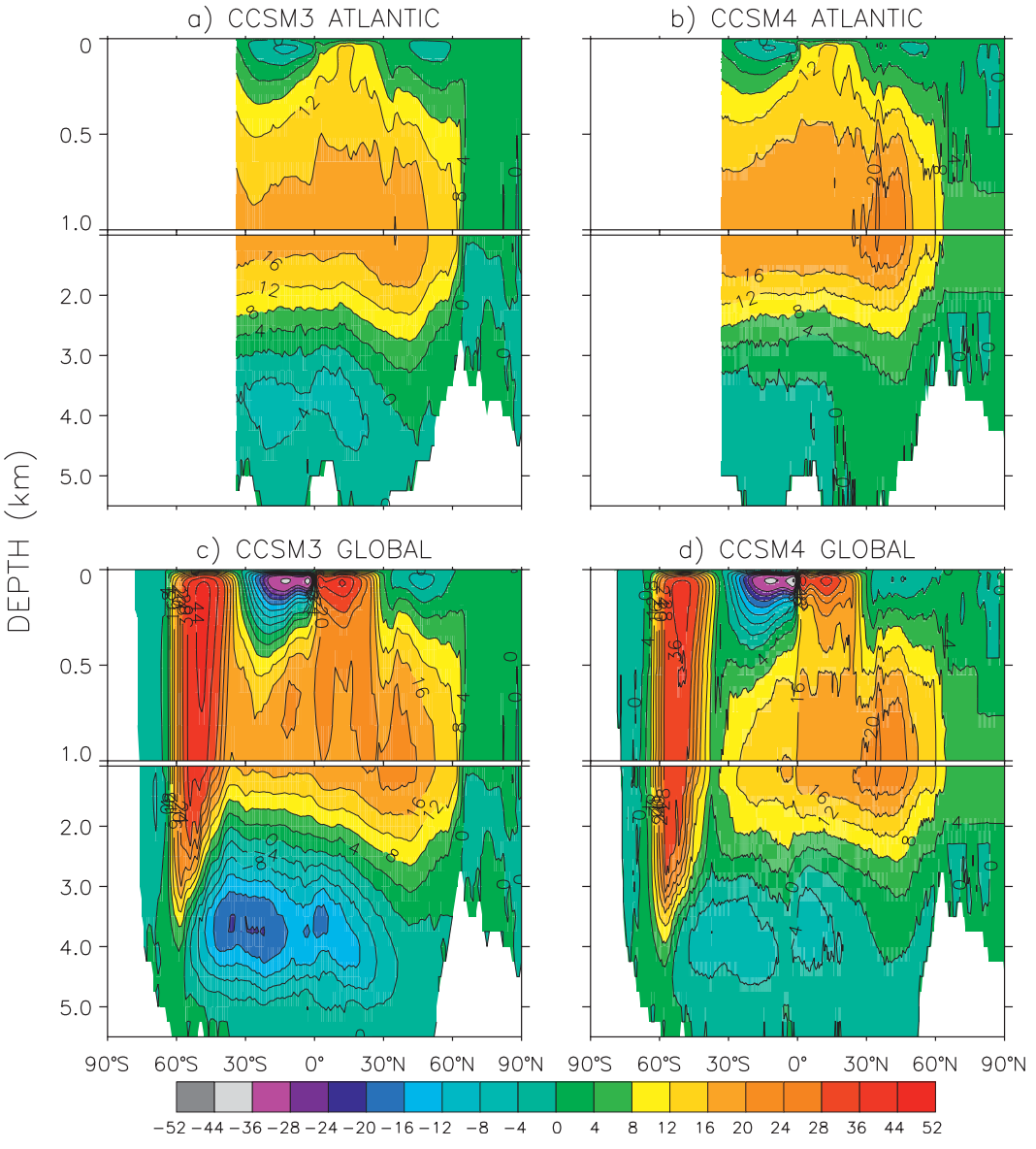

FIG. 2. North Atlantic MOC (Sv) for the (a) CCSM3 1870 control ⟨345–364⟩ and (b) CCSM4 1850 control ⟨871–900⟩, and global MOC for (c) CCSM3 1870 control and (d) CCSM4 1850 control.

5. Tropical Pacific climatology and variability

a. Precipitation

Figure 4 shows frequency versus daily precipitation rate over land in the tropics between 20°N and S. Results from one of the 1° and 2° CCSM4 and T85 CCSM3 twentieth-century runs are plotted with the observational estimates from the Global Precipitation Climatology Project (GPCP) and the Tropical Rainfall Measuring Mission (TRMM) satellite. Figure 4 shows that CCSM3 had far too few strong to very strong precipitation events compared to observations and had no events with a precipitation rate over 50 mm day^{-1}. In striking contrast, CCSM4 does produce a realistic number of strong to very strong precipitation events at both 1° and 2° resolutions. The reason for this improvement in CAM4 is the inclusion of deep convection effects in the momentum equation (Richter and Rasch 2008). This leads to much more realistic extreme precipitation events in CCSM4 than in CCSM3. Note that Wilcox and Donner (2007) also document improvements in the intensity distribution of precipitation resulting from changes to the cumulus parameterization in the Geophysical Fluid Dynamics Laboratory's Atmospheric Model (AM2) component.

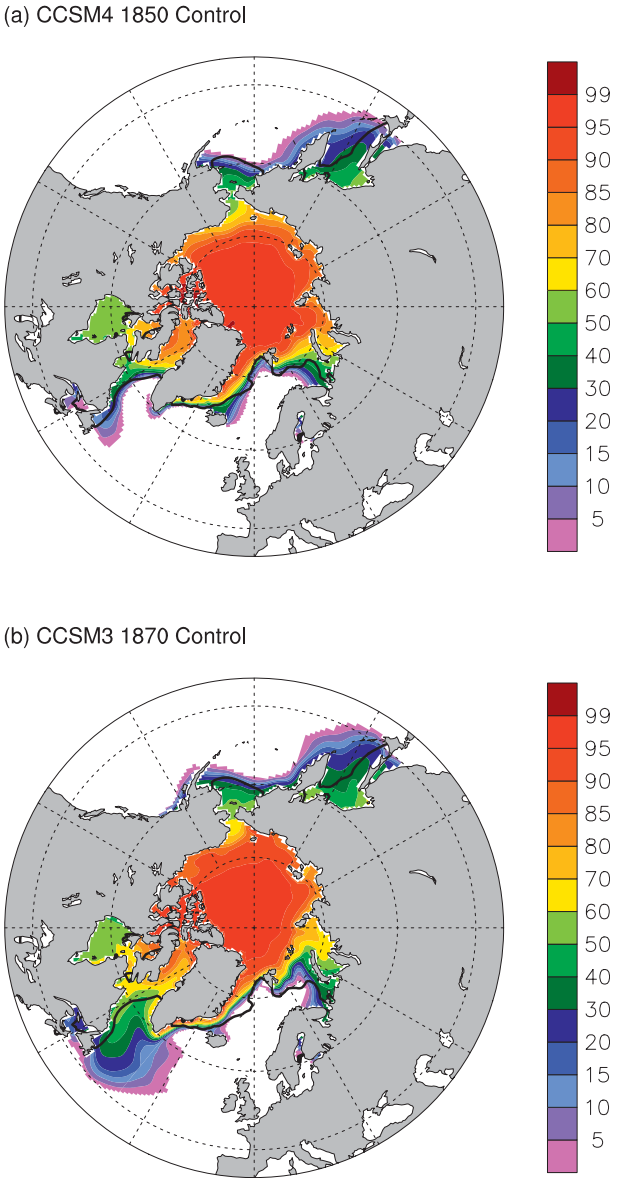

FIG. 3. Mean Arctic sea ice concentration (%) for the (a) CCSM4 1850 control and (b) CCSM3 1870 control; both ⟨871–900⟩. The black lines are the 10% mean concentration values from SSM/I observations (Cavalieri et al. 1996) ⟨1979–2000⟩.

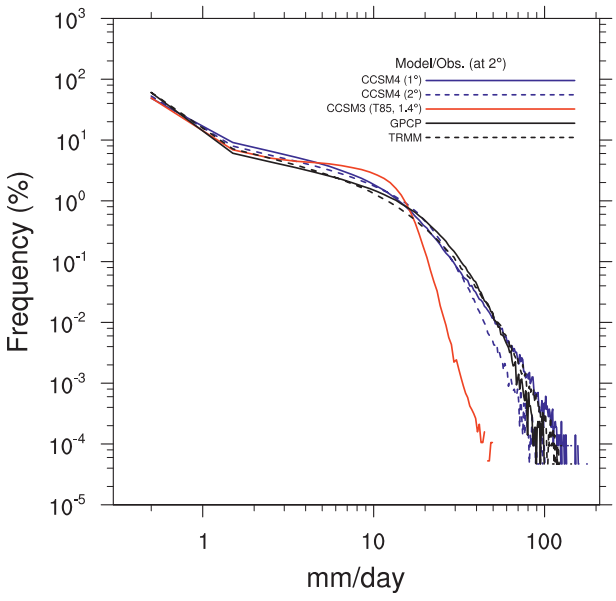

FIG. 4. Frequency (%) of daily precipitation rate over land between 20°N and S from GPCP and TRMM observations ⟨1999–2008⟩, from twentieth-century runs of CCSM4 at 1° and 2°, and from T85 CCSM3; all ⟨1990–99⟩. All data are interpolated to the 2° CAM4 grid.

However, the double intertropical convergence zone (ITCZ) problem remains. Figure 5 shows the annual mean precipitation compared to the GPCP climatology from twentieth-century runs of the 1° and 2° CCSM4 and T85 CCSM3 models. The GPCP climatology was used for this comparison because it is good in the tropics (Yin et al. 2004). The biases in 2° CCSM4 and CCSM3 are comparable, although the ITCZ in the central Pacific Ocean is located a bit farther north in the 2° CCSM4. Both models show the characteristic pattern of the double ITCZ problem with too much precipitation in the central Pacific near 5°S and too little precipitation in the west and central Pacific between 15° and 30°S. This characteristic pattern of precipitation bias still occurs in the 1° CCSM4, but its magnitude is reduced somewhat. The 1° CCSM4 model does show a smaller bias in the tropical Atlantic Ocean, but the dipole bias in the tropical Indian Ocean is as large as in the other models.

b. *Madden–Julian oscillation*

Figure 6a shows the structure of the first combined multivariate empirical orthogonal function (EOF) for observed 20–100-day bandpass-filtered anomalies of outgoing longwave radiation (OLR) and 200-hPa and 850-hPa winds between 15°N and S against longitude. This EOF is calculated as suggested by Waliser et al. (2009) and is representative of MJO variability. Figures 6b and 6c show the same EOF from a twentieth-century run of 1° CCSM4 and T85 CCSM3. Figure 6c clearly shows that CCSM3 had a very poor simulation of MJO variability because this first EOF has a very poor zonal structure that only accounts for 10.5% of the variance in this time band compared to 23.4% in the observations. Also, the phasing of the three variables is poor compared to observations in the east Indian and Pacific Oceans. The MJO variability is greatly improved in the CCSM4 twentieth-century run because of the much better EOF zonal structure, accounting for 19.1% of the total variance. In addition, the phasing of the variables across the east

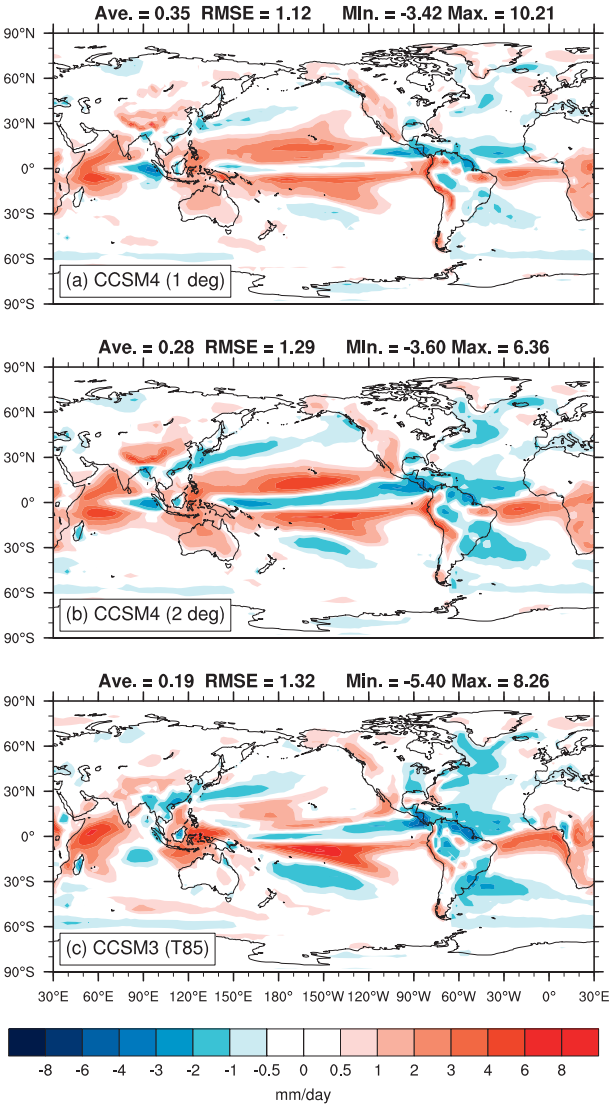

FIG. 5. Annual mean precipitation difference (mm day^{-1}) relative to the GPCP climatology for ⟨1970–99⟩ from twentieth-century runs using (a) 1° CCSM4, (b) 2° CCSM4, and (c) T85 CCSM3.

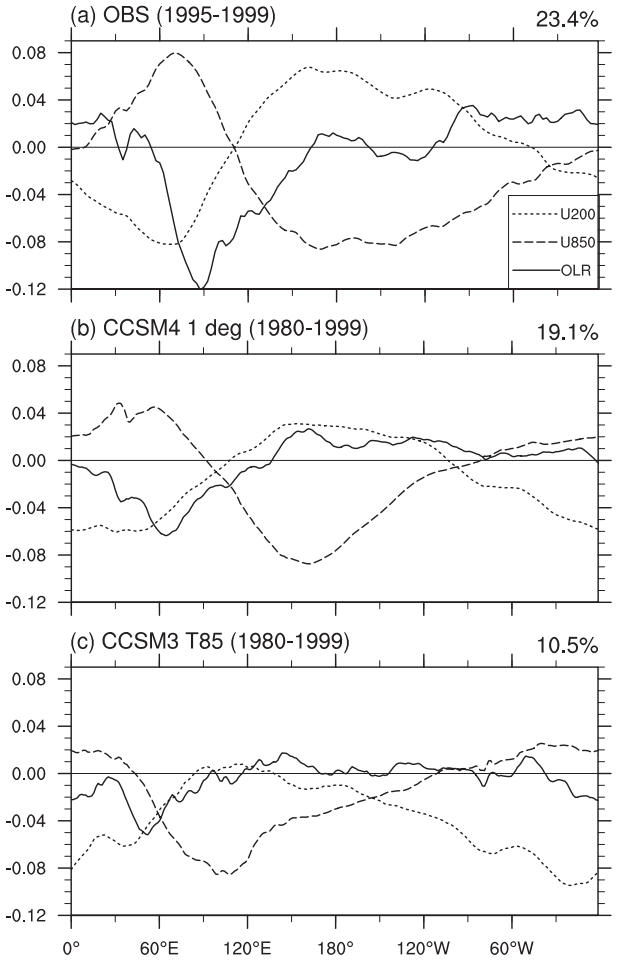

FIG. 6. Structure of the first combined multivariate EOF for observed 20–100-day bandpass-filtered anomalies of OLR and 200-hPa and 850-hPa winds between 15°N and S against longitude: (a) observations (NOAA OLR, NCEP winds), (b) the CCSM4 twentieth-century run, and (c) the CCSM3 twentieth-century run.

Indian and Pacific Oceans is much improved. This improvement in tropical variability results mainly from the change to use the dilute approximation in the plume calculation of the deep convection scheme (Neale et al. 2008).

c. *Mean and annual cycle of Pacific SSTs*

Figure 7 shows the mean and annual cycle of SSTs along the equator in the Pacific Ocean from observations and individual CCSM4 and CCSM3 twentieth-century runs. The mean SST in CCSM3 was cold by about 1.5°C across most of the Pacific, and this is much improved in CCSM4, which is warmer than the observations by only <0.4°C over most of the Pacific. The reasons for this improvement are slightly weaker easterly winds on the equator in CCSM4, which result in weaker equatorial upwelling, and stronger tropical instability wave activity in the ocean, which transports more heat onto the equator. Both model versions are warmer than reality at the western and eastern boundaries of the Pacific. The observations show a dominant annual cycle in SST in the eastern Pacific Ocean, with anomaly patterns propagating westward across the central Pacific. This has been difficult to reproduce well in climate models, and CCSM3 had an annual cycle with a strong semiannual component in the east Pacific and no consistent anomaly propagation. This is improved in CCSM4, which has a much smaller semiannual component in the east Pacific, and westward propagation of SST anomaly patterns at about the correct speed. The reasons for this

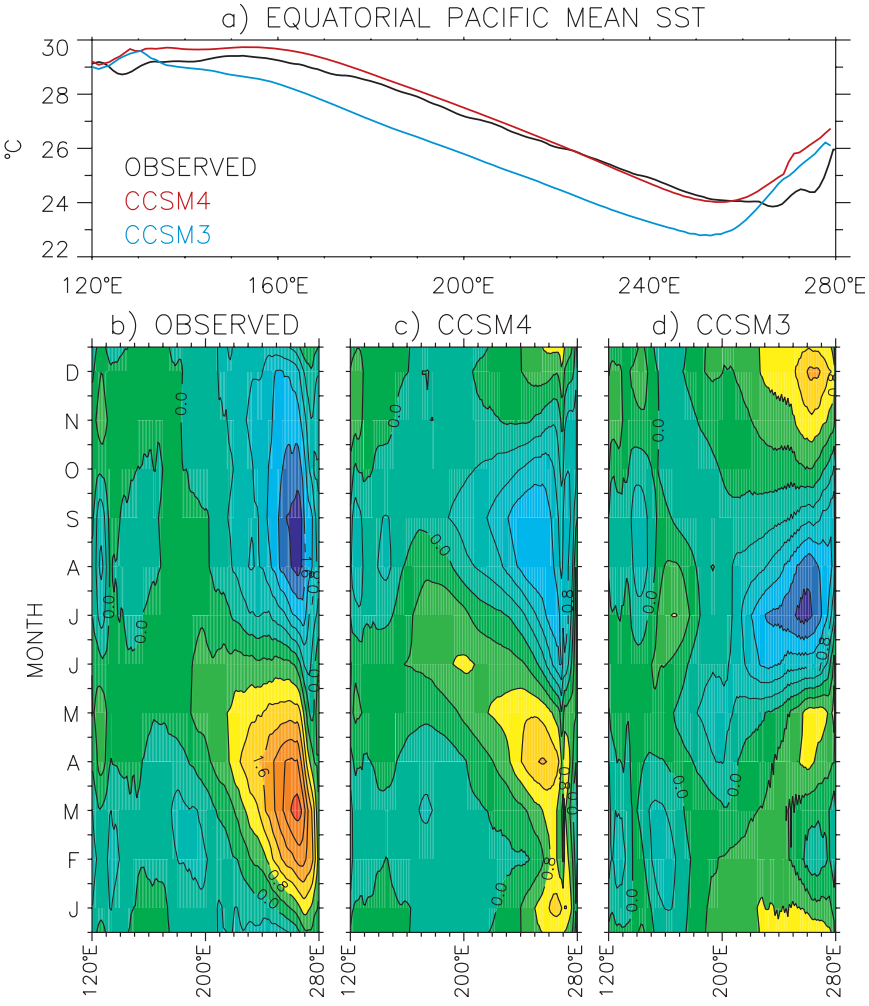

FIG. 7. (a) Mean SST (°C) along the equator in the Pacific Ocean and annual cycle of SST anomalies (CI = 0.4°C) for the (b) the Hurrell et al. (2008) data, (c) CCSM4 twentieth-century run, and (d) CCSM3 twentieth-century run; all ⟨1970–99⟩.

improvement are a combination of a better mean state and an improved simulation of surface currents due to a better wind stress simulation, especially just north of the equator in the east Pacific. However, there is still room for improvement, as the amplitude of the annual SST cycle in the east Pacific is much smaller in CCSM4 than in observations.

d. El Niño–Southern Oscillation

Figure 8 shows the variance spectra of Niño-3 monthly SST anomalies from Hurrell et al.'s (2008) data and the CCSM4 1850 and CCSM3 1870 control runs. The centuries chosen from the control runs have ENSO amplitudes representative of the full control run amplitudes. The CCSM3 spectrum is dominated by a fairly narrow peak at 2 yr. This resulted from its ENSO having positive and negative phases that very regularly followed each other a year later. This is at odds with observations where the frequency spectrum has a broad peak with variability between 3 and 7 yr. This very poor representation of ENSO was noted in Collins et al. (2006) as one of the worst aspects of all previous CCSM versions. Figure 8 shows that the ENSO frequency spectrum distribution in CCSM4 is a huge improvement over CCSM3; it has very little power at 2 yr and variability between 3 and 6 yr with a peak at 4 yr. This improvement was the direct result of the two changes to the CAM4 deep convection scheme documented in Richter and Rasch (2008) and Neale et al. (2008). The reasons for this improvement are analyzed in detail in Neale et al. (2008), and their conclusion states, "Including convective momentum transport in the convection parameterization weakened the trades and the off-equatorial wind response to an El Niño event; allowing for convective

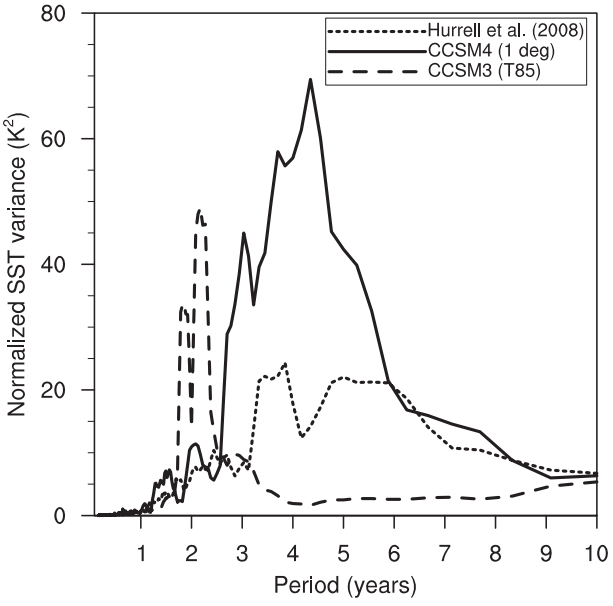

FIG. 8. Variance spectra of monthly mean Niño-3 SST anomalies from the Hurrell et al. (2008) data ⟨1901–2000⟩, the CCSM4 1850 control ⟨401–500⟩, and the CCSM3 1870 control ⟨801–900⟩.

plume entrainment strengthened MJO activity. The first process weakened the delayed oscillator, which produces the overly regular ENSO in CCSM3; the second process then added a mechanism for maintaining El Niño events.'' Guilyardi et al. (2009) say that the changes documented in Neale et al. (2008) strengthen both the Bjerknes feedback and the heat flux feedback compared to CCSM3.

The CCSM4 ENSO variability is not perfect because Fig. 8 shows that the amplitude is considerably larger than in the Hurrell et al. (2008) data. However, the model ENSO amplitude has quite a lot of variability, and a century in the control run can be found where the amplitude is considerably smaller, and compares better with the data. Another aspect of the much better CCSM4 ENSO is documented in Fig. 9, which shows the correlation of monthly mean Niño-3 SST anomalies with global SST anomalies from the Hurrell et al. (2008) data, CCSM4 1850 control, and CCSM3 1870 control. The figure shows that CCSM4 has a much more realistic meridional width to the positive correlations in the central and eastern tropical Pacific. Also, the horseshoe pattern of negative correlations in the western tropical Pacific that stretches into the midlatitudes of both hemispheres in the Pacific is greatly improved. However, it is stronger than observed in the west Pacific between the equator and 20°N, probably because of the too large ENSO amplitude. These two figures document the greatly improved ENSO variability in CCSM4 compared to CCSM3, and further analysis of CCSM4 ENSO is in Deser et al. (2011, manuscript submitted to *J. Climate*).

6. Land climatology and variability

a. Land water storage

Figure 10 shows the difference in mean soil and snow water content between the boreal spring, March–May (MAM), and boreal fall, September–November (SON), from Gravity Recovery And Climate Experiment (GRACE) satellite data and the CCSM4 and CCSM3 control runs. In the tropics the GRACE data shows a dipole pattern with respect to the equator, which results from the migration of the monsoons from south of the equator in boreal winter to north of the equator in boreal summer. The CCSM4 reproduces both this pattern and the magnitude of up to ±300 mm rather well. In contrast, the magnitude in CCSM3 was only up to ±100 mm, which was a factor of 3 too small. In addition, the magnitude of the land-water storage compares better with the GRACE data in CCSM4 over large areas of Canada and Russia, although the magnitude is too large in coastal Alaska and western Russia due to excessively deep spring snowpacks. The improvement in CCSM4 is due to several new hydrology and snow parameterizations that act together to produce more realistic behavior. Among the most influential sources of this improvement are reduced canopy interception, which permits more water to reach the ground; reduced runoff as a consequence of the incorporation of a simple prognostic groundwater model; improved permeability of frozen soil; and more restrictive controls on ground evaporation (Oleson et al. 2008). The new land model has a much improved capacity to store soil water from one season to the next, which improves the simulation of latent heat flux in the dry and transition seasons. For example, the Amazon basin latent heat flux in CCSM4 remains high throughout the dry season as observed, whereas in CCSM3 the latent heat flux in the dry season drops off significantly and unrealistically.

b. Land surface temperatures

Figure 11 shows the annual mean bias and rms error (RMSE) in land surface temperature from CCSM4 and CCSM3 compared to observations. The globally averaged mean bias of −0.17°C in CCSM4 is smaller than the −0.28°C in CCSM3, although this improved mean is partially because of a larger area of positive bias up to 4°C in eastern Europe and western Russia in CCSM4. This can be seen as a large red area in Fig. 11c: the green (red) shading shows areas where the CCSM4 (CCSM3) mean bias is smaller compared to observations, and gray

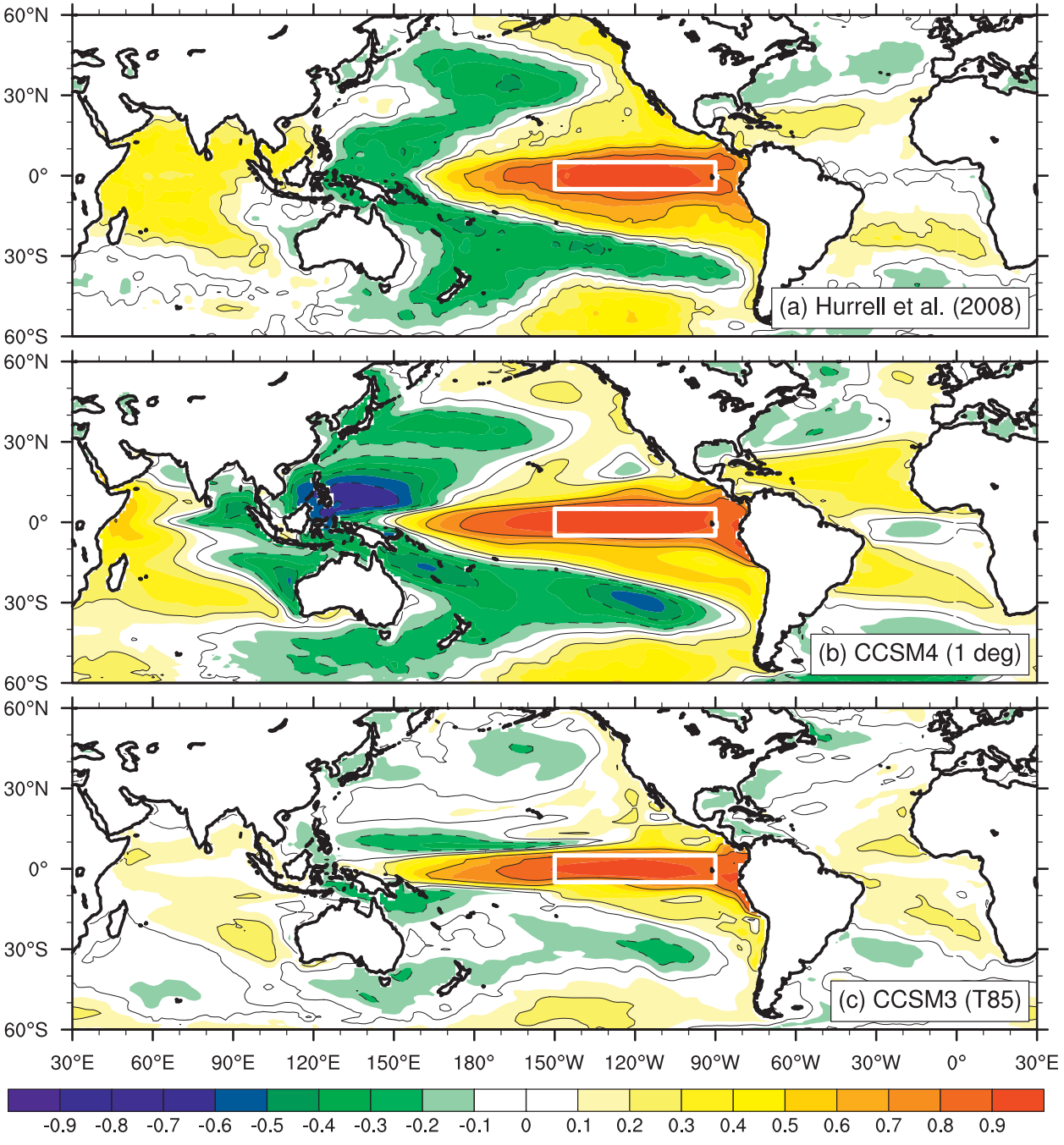

FIG. 9. Correlation of monthly mean Niño-3 SST anomalies with global SST anomalies for the (a) Hurrell et al. (2008) data ⟨1901–2000⟩, (b) CCSM4 1850 control ⟨401–500⟩, and (c) CCSM3 1870 control ⟨801–900⟩.

shading shows areas where the models have the same bias within one standard deviation. Figure 11f shows areas where the CCSM4 (CCSM3) RMSE is smaller in green (red) shading. The large area of green shows that CCSM4 has a smaller RMSE than CCSM3 in many areas across the continents, especially in the high latitudes of the Northern Hemisphere. This results in a 10% reduction in the global RMSE in CCSM4 to 2.71°C compared to CCSM3. It is difficult to pinpoint the reasons for changes in surface land temperatures because they depend on both atmosphere and land components. However, inclusion of the Snow, Ice, and Aerosol Radiative (SNICAR) model has improved the realism of land snow and radiation physics.

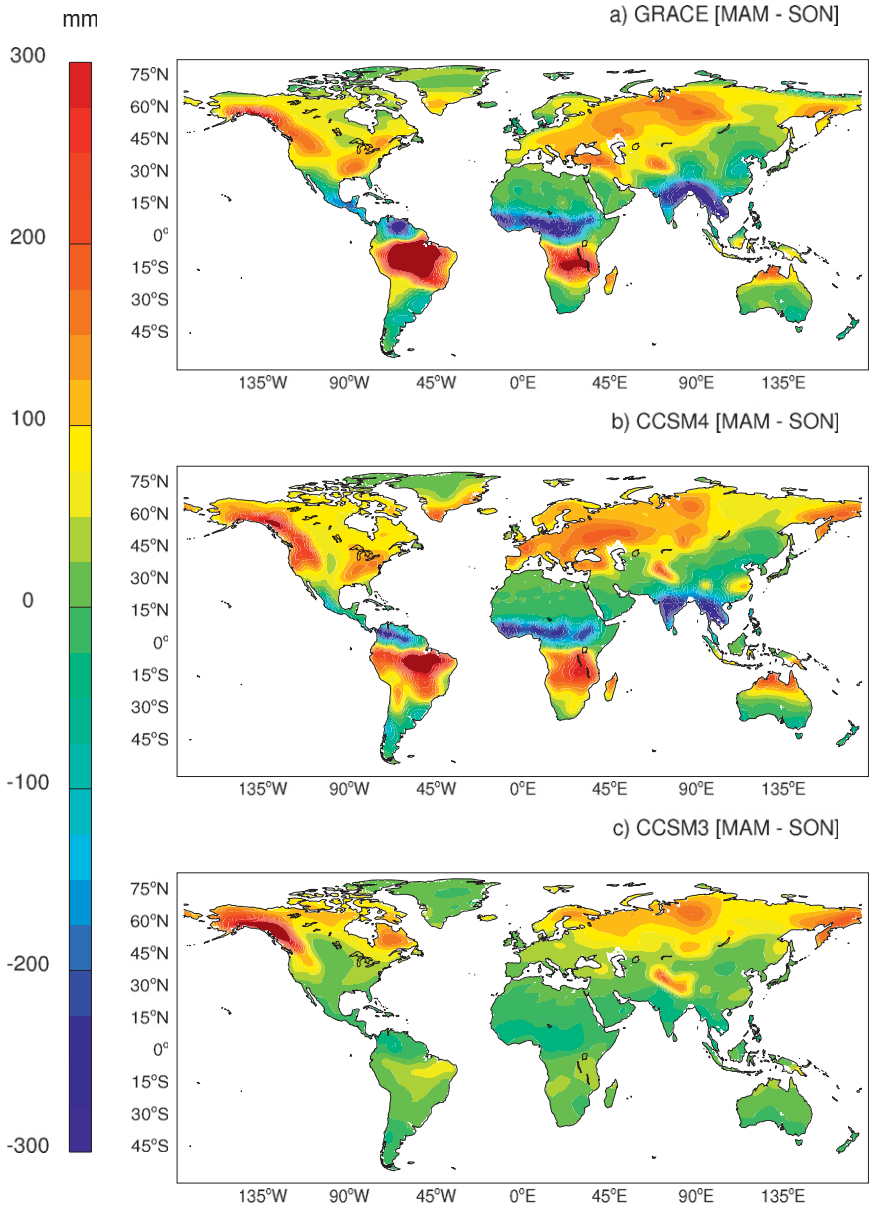

FIG. 10. Difference in mean soil water content (mm) between boreal spring (MAM) and boreal fall (SON) for the (a) GRACE data (Swenson and Milly 2006) ⟨2002–08⟩, (b) CCSM4 1850 control, and (c) CCSM3 1870 control, both ⟨871–900⟩.

7. Climate evolution of twentieth-century runs

a. Globally averaged surface temperature

Figure 12 shows time series of the globally averaged surface temperature anomaly from observations and the ensemble mean from five twentieth-century runs of CCSM3 and CCSM4, plus the CCSM4 ensemble spread. The model results track the data quite well up to 1970, except for three instances. The first two are when the models have a large dip in temperature due to the Krakatoa eruption in 1883 and volcanic eruptions in 1902 that are not apparent in the data at all, and the third is when the models do not show a temperature decrease in the 1940s that is clearly evident in the Hadley Centre–Climate Research Unit Temperature Anomalies (HadCRUT3) data. These discrepancies have been present in all twentieth-century runs done with CCSM. After 1970, the CCSM4 surface temperature increases faster than the data so that by 2005 the model anomaly is 0.4°C larger than the observed anomaly. This too large increase in surface temperature occurs in all CCSM4 twentieth-century runs. It is interesting to note however,

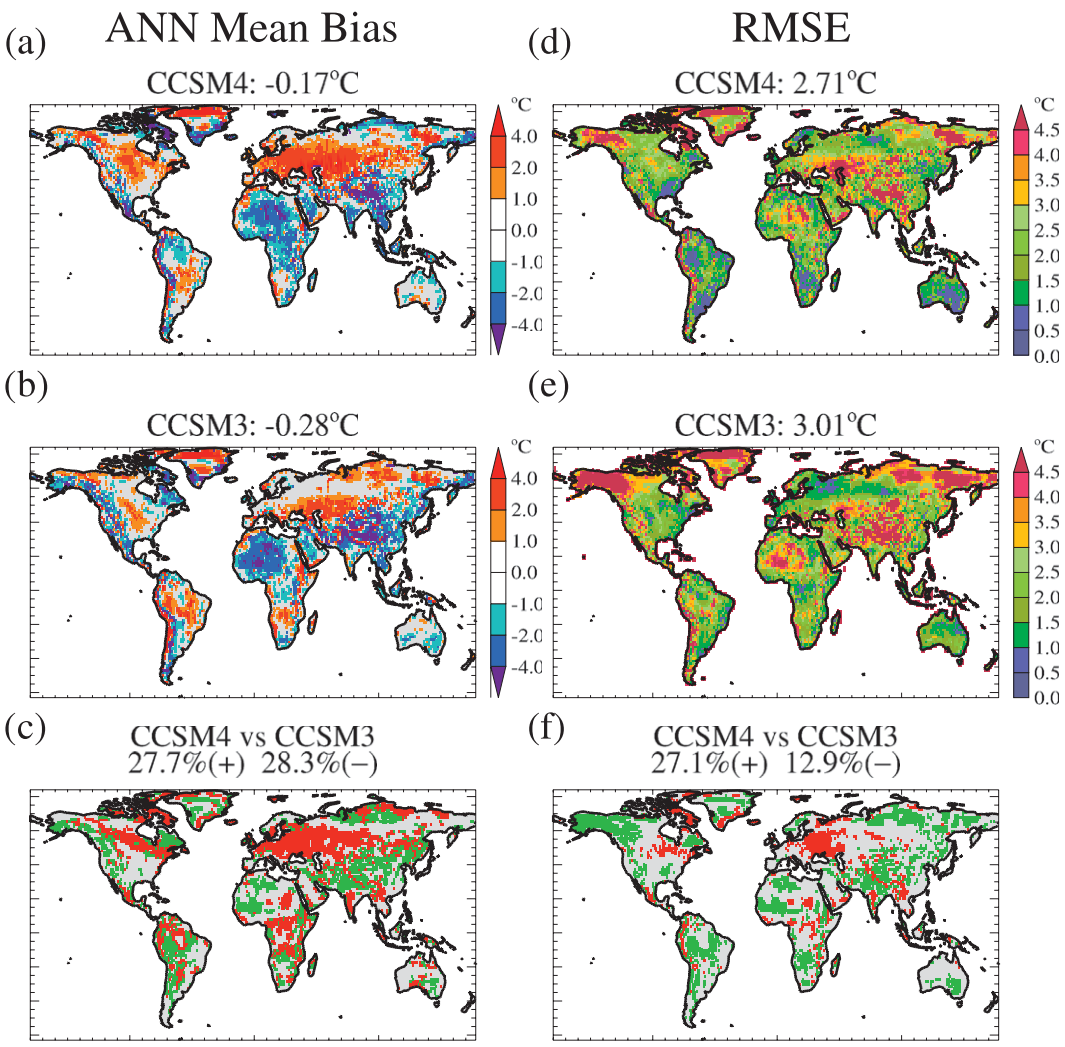

FIG. 11. Differences of model land surface air temperature (°C) from observations (Willmott and Matsuura 2000); all ⟨1950–99⟩. Annual mean bias for the (a) CCSM4 twentieth-century run, (b) CCSM3 twentieth-century run, and (c) for CCSM4 vs CCSM3. RMSEs for (d) CCSM4, (e) CCSM3, and (f) CCSM4 vs CCSM3. In (c) and (f) green (red) areas are where CCSM4 (CCSM3) is in better agreement with the observations; gray areas indicate no difference.

that, if CCSM4 twentieth-century runs had ended in 2000 rather than 2005, then the comparison would have looked much better. Over the last 5 yr of the run, the model temperature increased significantly whereas the earth's temperature over that period did not change much at all. However, it is clear from Fig. 12 that the CCSM4 surface temperature increases faster than both the observations and CCSM3.

There are several possibilities for the differences between the models and reality. Neither model includes the indirect effects of aerosols, which have cooled the earth somewhat over the twentieth century. This implies that both models should warm faster than the observations, and the fact that CCSM3 did not do so suggests that probably the cooling effect of volcanoes is too strong in that model. Volcanoes are implemented in exactly the same way in both models, and Fig. 12 clearly shows the quite large temperature response to large eruptions that is not reflected in the observations. This could possibly be a problem with the temperature reconstruction, which has only sparse data in the early part of the record, and a temperature drop might show up better using data just over land. However, there are other possibilities for model errors, such as a poor representation of the direct effect of aerosols or the climate sensitivity is incorrect. In addition, the heat uptake by the ocean may be too small, although Gent et al. (2006) show that the CCSM3 heat uptake is larger than observations suggest, and uptake of chlorofluorocarbon-11 agrees well with observations. It is very difficult to say definitively which of

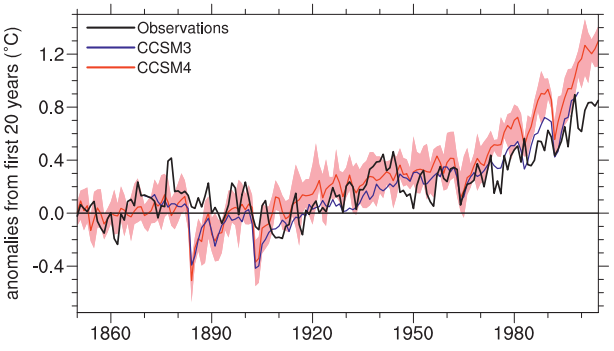

FIG. 12. Time series of globally averaged surface temperature anomaly (°C) from the HadCRUT3 data (Brohan et al. 2006), CCSM3, and CCSM4 twentieth-century ensemble means. Each time series is calculated relative to its mean of the first 20 yr. Shading shows the maximum and minimum of the CCSM4 ensemble spread.

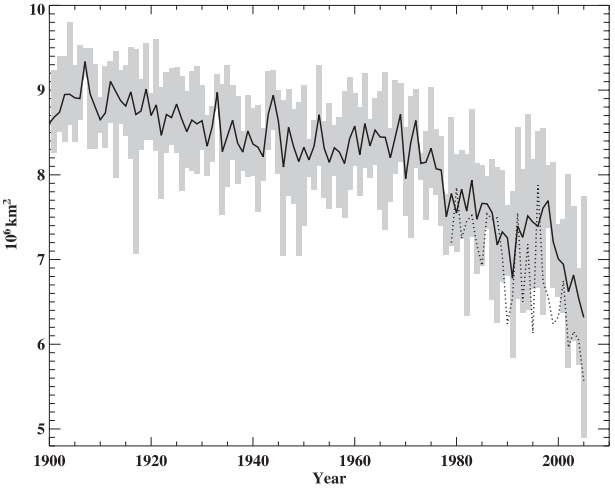

FIG. 13. Time series of Arctic sea ice extent (10^6 km^2) in September from the observed NSIDC Sea Ice Index (Fetterer et al. 2009) (dotted) for 1979–2009 and the CCSM4 twentieth-century ensemble mean (solid), with the shading showing the maximum and minimum of the ensemble spread.

these possibilities causes the CCSM4 too large surface temperature increase over the twentieth century.

The average heat gain at the TOA over the entire duration of the CCSM4 twentieth-century ensemble runs is 0.254 W m^{-2} compared to the drift in the 1850 control run. By 2005, the average heat input is 1.15 W m^{-2}, which is slightly larger than the 0.9 ± 0.15 W m^{-2} that observations of the heat imbalance for 2000–04 suggest (Hansen et al. 2005; Trenberth et al. 2009). This excess rate of heat gain, and the consequent larger surface temperature increase in CCSM4 compared to CCSM3, is most likely because it has a higher climate sensitivity. The transient climate sensitivity of the 1° version is 1.72°C compared to 1.50°C for the CCSM3 T85 version (Kiehl et al. 2006). The CCSM4 1° version equilibrium climate sensitivity due to a doubling of CO_2 is 3.2° ± 0.1°C (Bitz et al. 2011, manuscript submitted to *J. Climate*, hereafter B11), whereas the T85 CCSM3 sensitivity is 2.7° ± 0.1°C (Kiehl et al. 2006). The reasons for this increase in CCSM4 equilibrium climate sensitivity are analyzed in detail in B11.

b. *September Arctic sea ice extent*

Figure 13 shows the observed Arctic sea ice extent in September and the ensemble mean of the CCSM4 twentieth-century runs from 1900 to 2005, with the shading showing the range of the CCSM4 ensemble. The ensemble mean shows some variability in this extent with a small decreasing trend up to about 1975 and then a much larger decreasing trend afterward that is quite close to the observed downward trend. The 1979–2005 trends from the different ensemble members bracket the observed trend over this period, as was the case for CCSM3. In addition, the standard deviation in each run between 1979 and 2005 is also comparable to the observations. The CCSM project has made this comparison a very high priority so that the model can be used to make future projections of the Arctic sea ice. Plausible future projections of Arctic sea ice from CCSM3 are analyzed in Holland et al. (2006).

8. Summary and conclusions

The first conclusion is that sections 4–7 show that there are many improvements in CCSM4 simulations compared to those from CCSM3. The most important improvements are in the frequency of ENSO variability and the SST correlations with the whole Pacific Ocean, shown in Figs. 8 and 9. The changes to the deep convection scheme in the atmosphere component, documented in Richter and Rasch (2008) and Neale et al. (2008), also improve the representation of the frequency distribution of tropical precipitation and MJO variability, as shown in Figs. 4 and 6. Higher horizontal atmospheric resolution and vertical resolution in the upper ocean help to reduce the SST errors in the main upwelling regions, shown in Fig. 1, and improve the mean and annual cycle of SST along the equator in the eastern Pacific, shown in Fig. 7. The new parameterization of overflows in the ocean component improves the penetration of the North Atlantic MOC, shown in Fig. 2, and the path of the Gulf Stream.

Changes in the land component lead to improved water storage over the annual cycle, shown in Fig. 10, which leads to a better latent heat flux into the atmosphere and river runoff into the ocean. The land component changes also helped to reduce the RMSE biases in surface

temperature, shown in Fig. 11. Therefore, CCSM4 has a much better representation of extreme events, such as heat waves and very heavy rainfall, than did CCSM3. Figure 3 shows the improvement in Arctic sea ice concentration in CCSM4, where the southern Labrador Sea is ice free. In addition, the sea ice thickness distribution in both hemispheres is obtained in CCSM4 using much more realistic sea ice albedos, because the CCSM3 bias of 40–50 W m^{-2} too low downward solar radiation in the Arctic summer has been almost eliminated in CCSM4. The CCSM4 twentieth-century ensemble compares well with observations of the declining September Arctic sea ice extent over 1979–2005, as shown in Fig. 13.

The second conclusion is that CCSM4 still has significant biases that need to be worked on and improved. Figure 5 shows that the improvements to deep convection in CAM4 have not eliminated the double ITCZ problem, even in the 1° version. Gent et al. (2010) show that the 0.5°-resolution version of CCSM3.5 also had a double ITCZ so that just increasing the atmospheric resolution may not eliminate the double ITCZ; further parameterization improvements are almost certainly required. The CCSM4 still has biases compared to observations in the latitudinal distribution of both the shortwave and longwave cloud forcing (not shown). Unfortunately, these biases do not get smaller when the higher horizontal resolution of 0.5° is used in the atmospheric component because the cloud distribution in CCSM4 is not sufficiently accurate compared to observations. There is still too much low cloud in the Arctic region, despite including the freeze-dry parameterization of Vavrus and Waliser (2008). Figure 11 shows room for improvement in the surface temperature over the continents, which has significant areas where the mean bias is >2°C compared to the Willmott and Matsuura (2000) observations.

The third conclusion is that the missing indirect effects of aerosols in CCSM4 is very likely a major factor causing the larger increase in globally averaged surface temperature over the twentieth century than in observations, shown in Fig. 12. However, there are other possibilities for this too large increase, such as a poor representation of the direct effect of aerosols, the ocean heat uptake is too small, or the model climate sensitivity is too large. The absence of aerosol indirect effects means that projections of future temperature rise due to increased CO_2 and other greenhouse gases will be larger than if CCSM4 did include the aerosol indirect effects. These last two conclusions clearly point out the necessity of an improved atmosphere component that includes a better representation of cloud physics and aerosols that allows for feedback of the indirect effects of aerosols. A new version of CAM that includes these processes, and other improved parameterizations, has been under development for some time and is ready to be incorporated into CCSM. Results using this new atmosphere component will be documented in the very near future.

Acknowledgments. This paper is dedicated to the memory of Byron Boville, who worked on the development of all CCSM versions, but did not live long enough to see CCSM4 completed. Jay Fein has been a very strong supporter of the CCSM project since its inception. Thanks and best wishes to Jay upon his retirement from the atmospheric sciences section at the National Science Foundation, which sponsors NCAR and the CCSM Project. The project is also sponsored by the U.S. Department of Energy (DOE). Thanks are also due to the many other software engineers and scientists who worked on developing CCSM4, and to the Computational and Information Systems Laboratory at NCAR, which provided the computing resources through the Climate Simulation Laboratory. Hunke was supported within the Climate, Ocean and Sea Ice Modeling project at Los Alamos National Laboratory, which is funded by the Biological and Environmental Research division of the DOE Office of Science. The Los Alamos National Laboratory is operated by the DOE National Nuclear Security Administration under Contract DE-AC52-06NA25396. Rasch was supported by the DOE Office of Science, Earth System Modeling Program, which is part of the DOE Climate Change Research Program. The Pacific Northwest National Laboratory is operated for DOE by Battelle Memorial Institute under Contract DE-AC06-76RLO 1830. Worley was supported by the Climate Change Research Division of the Office of Biological and Environmental Research and by the Office of Advanced Scientific Computing Research, both in the DOE Office of Science, under Contract DE-AC05-00OR22725 with UT-Batelle, LLC.

REFERENCES

Ammann, C. M., G. A. Meehl, W. M. Washington, and C. Zender, 2003: A monthly and latitudinally varying volcanic forcing dataset in simulations of 20th century climate. *Geophys. Res. Lett.,* **30,** 1657, doi:10.1029/2003GL016875.

Bernie, D. J., S. J. Woolnough, J. M. Slingo, and E. Guilyardi, 2005: Modeling diurnal and intraseasonal variability of the ocean mixed layer. *J. Climate,* **18,** 1190–1202.

Boville, B. A., and P. R. Gent, 1998: The NCAR Climate System Model, version one. *J. Climate,* **11,** 1115–1130.

Briegleb, B. P., and B. Light, 2007: A delta-Eddington multiple scattering parameterization for solar radiation in the sea ice component of the Community Climate System Model. NCAR Tech. Note 472 + STR, 100 pp.

Brohan, P., J. J. Kennedy, I. Harris, S. F. Tett, and P. D. Jones, 2006: Uncertainty estimates in regional and global observed

temperature changes: A new dataset from 1850. *J. Geophys. Res.,* **111,** D12106, doi:10.1029/2005JD006548.

Cavalieri, D., C. Parkinson, P. Gloersen, and H. J. Zwally, 1996: Sea ice concentrations from Nimbus-7 SMMR and DMSP SSM/I passive microwave data; updated. National Snow and Ice Data Center, Boulder, CO. [Available online at http://nsidc.org/data/nsidc-0051.html.]

Collins, W. D., and Coauthors, 2006: The Community Climate System Model version 3 (CCSM3). *J. Climate,* **19,** 2122–2143.

Danabasoglu, G., and J. Marshall, 2007: Effects of vertical variations of thickness diffusivity in an ocean general circulation model. *Ocean Modell.,* **18,** 122–141.

——, W. G. Large, J. J. Tribbia, P. R. Gent, B. P. Briegleb, and J. C. McWilliams, 2006: Diurnal coupling in the tropical oceans of CCSM3. *J. Climate,* **19,** 2347–2365.

——, R. Ferrari, and J. C. McWilliams, 2008: Sensitivity of an ocean general circulation model to a parameterization of near-surface eddy fluxes. *J. Climate,* **21,** 1192–1208.

——, S. Bates, B. Briegleb, S. Jayne, M. Jochum, W. Large, S. Peacock, and S. Yeager, 2011a: The CCSM4 ocean component. *J. Climate,* in press.

——, W. G. Large, and B. P. Briegleb, 2011b: Climate impacts of parameterized Nordic Sea overflows. *J. Geophys. Res.,* **115,** C11005, doi:10.1029/2010JC006243.

Fetterer, F., K. Knowles, W. Meier, and M. Savoie, 2009: Sea ice index. National Snow and Ice Data Center, Boulder, CO. [Available online at http://nsidc.org/data/g02135.html.]

Flanner, M. G., and C. S. Zender, 2006: Linking snowpack microphysics and albedo evolution. *J. Geophys. Res.,* **111,** D12208, doi:10.1029/2005JD006834.

Fox-Kemper, B., R. Ferrari, and R. Hallberg, 2008: Parameterization of mixed layer eddies. Part I: Theory and diagnosis. *J. Phys. Oceanogr.,* **38,** 1145–1165.

Gent, P. R., F. O. Bryan, G. Danabasoglu, K. Lindsay, D. Tsumune, M. W. Hecht, and S. C. Doney, 2006: Ocean chlorofluorocarbon and heat uptake during the twentieth century in the CCSM3. *J. Climate,* **19,** 2366–2381.

——, S. G. Yeager, R. B. Neale, S. Levis, and D. A. Bailey, 2010: Improvements in a half degree atmosphere/land version of the CCSM. *Climate Dyn.,* **34,** 819–833, doi:10.1007/s00382-009-0614-8.

Guilyardi, E., P. Braconnot, F. F. Jin, S. T. Kim, M. Kolasinski, T. Li, and I. Musat, 2009: Atmosphere feedbacks during ENSO in a coupled GCM with a modified atmospheric convection scheme. *J. Climate,* **22,** 5698–5718.

Hansen, J., and Coauthors, 2005: Earth's energy imbalance: Confirmation and implications. *Science,* **308,** 1431–1435.

Heald, C. L., and Coauthors, 2008: Predicted change in global secondary organic aerosol concentrations in response to future climate, emissions, and land use change. *J. Geophys. Res.,* **113,** D05211, doi:10.1029/2007JD009092.

Holland, M. M., C. M. Bitz, and B. Tremblay, 2006: Future abrupt reductions in the summer Arctic sea ice. *Geophys. Res. Lett.,* **33,** L23503, doi:10.1029/2006GL028024.

——, D. A. Bailey, B. P. Briegleb, B. Light, and E. Hunke, 2011: Improved sea ice shortwave radiation physics in CCSM4: The impact of melt ponds and aerosols on Arctic sea ice. *J. Climate,* in press.

Hunke, E. C., and W. H. Lipscomb, 2008: CICE: The Los Alamos sea ice model user's manual, version 4. Los Alamos National Laboratory Tech. Rep. LA-CC-06-012, 76 pp.

Hurrell, J. W., J. J. Hack, D. Shea, J. M. Caron, and J. Rosinski, 2008: A new sea surface temperature and sea ice boundary dataset for the Community Atmosphere Model. *J. Climate,* **21,** 5145–5153.

Hurtt, G. C., and Coauthors, 2006: The underpinnings of land-use history: Three centuries of global gridded land-use transitions, wood-harvest activity, and resulting secondary lands. *Global Change Biol.,* **12,** 1208–1229.

Jayne, S. R., 2009: The impact of abyssal mixing parameterizations in an ocean general circulation model. *J. Phys. Oceanogr.,* **39,** 1756–1775.

Jochum, M., G. Danabasoglu, M. M. Holland, Y. O. Kwon, and W. G. Large, 2008: Ocean viscosity and climate. *J. Geophys. Res.,* **113,** C06017, doi:10.1029/2007JC004515.

Kiehl, J. T., and P. R. Gent, 2004: The Community Climate System Model, version 2. *J. Climate,* **17,** 3666–3682.

——, C. A. Shields, J. J. Hack, and W. D. Collins, 2006: The climate sensitivity of the Community Climate System Model version 3 (CCSM3). *J. Climate,* **19,** 2584–2596.

Lamarque, J. F., and Coauthors, 2010: Historical (1850–2000) gridded anthropogenic and biomass burning emissions of reactive gases and aerosols: Methodology and application. *Atmos. Chem. Phys. Discuss.,* **10,** C922–C926.

Lawrence, D. M., and Coauthors, 2011a: Parameterization improvements and functional and structural advances in version 4 of the Community Land Model. *J. Adv. Model. Earth Syst.,* **3,** M03001, doi:10.1029/2011MS000045.

Lawrence, P. J., and T. N. Chase, 2007: Representing a new MODIS consistent land surface in the Community Land Model (CLM3.0). *J. Geophys. Res.,* **112,** G01023, doi:10.1029/2006JG000168.

Lean, J., G. Rottman, J. Harder, and G. Kopp, 2005: SORCE contributions to new understanding of global change and solar variability. *Sol. Phys.,* **230,** 27–53.

Lin, S. J., 2004: A ''vertically Lagrangian'' finite-volume dynamical core for global models. *Mon. Wea. Rev.,* **132,** 2293–2307.

Lipscomb, W. H., E. C. Hunke, W. Maslowski, and J. Jakacki, 2007: Improving ridging schemes for high-resolution sea ice models. *J. Geophys. Res.,* **112,** C03S91, doi:10.1029/2005JC003355.

Neale, R. B., J. H. Richter, and M. Jochum, 2008: The impact of convection on ENSO: From a delayed oscillator to a series of events. *J. Climate,* **21,** 5904–5924.

Oleson, K. W., and Coauthors, 2008: Improvements to the Community Land Model and their impact on the hydrological cycle. *J. Geophys. Res.,* **113,** G01021, doi:10.1029/2007JG000563.

Orsi, A. H., G. C. Johnson, and J. L. Bullister, 1999: Circulation, mixing, and production of Antarctic bottom water. *Prog. Oceanogr.,* **43,** 55–109.

Richter, J. H., and P. J. Rasch, 2008: Effects of convective momentum transport on the atmospheric circulation in the Community Atmosphere Model, version 3. *J. Climate,* **21,** 1487–1499.

Smith, R. D., and Coauthors, 2010: The Parallel Ocean Program (POP) reference manual. Los Alamos National Laboratory Tech. Rep. LAUR-10-01853, 140 pp.

Stockli, R., and Coauthors, 2008: Use of FLUXNET in the Community Land Model development. *J. Geophys. Res.,* **113,** G01025, doi:10.1029/2007JG000562.

Swenson, S., and P. C. Milly, 2006: Systematic climate model errors in seasonal water storage on continents revealed by satellite gravimetry. *Water Resour. Res.,* **42,** W03201, doi:10.1029/2005WR004628.

Thornton, P. E., J. F. Lamarque, N. A. Rosenbloom, and N. M. Mahowald, 2007: Influence of carbon/nitrogen cycle coupling on land model response to CO_2 fertilization and climate

variability. *Global Biogeochem. Cycles,* **21,** GB4018, doi:10.1029/2006GB002868.

Trenberth, K. E., J. T. Fasullo, and J. T. Kiehl, 2009: Earth's global energy budget. *Bull. Amer. Meteor. Soc.,* **90,** 311–323.

Vavrus, S., and D. Waliser, 2008: An improved parameterization for simulating Arctic cloud amount in the CCSM3 climate model. *J. Climate,* **21,** 5673–5687.

Waliser, D., and Coauthors, 2009: MJO simulation diagnostics. *J. Climate,* **22,** 3006–3030.

Wilcox, E. M., and L. J. Donner, 2007: The frequency of extreme rain events in satellite observations and an atmospheric circulation model. *J. Climate,* **20,** 53–69.

Willmott, C. J., and K. Matsuura, 2000: Terrestrial air temperature and precipitation: Monthly and annual climatologies. [Available online at http://climate.geog.udel.edu/-climate.]

Yin, X., A. Gruber, and P. Arkin, 2004: Comparison of the GPCP and CMAP merged guage–satellite monthly precipitation products for the period 1979–2001. *J. Hydrometeor.,* **5,** 1207–1222.